Journal of ELECTRICAL ENGINEERING, VOL. 55, NO. 7-8, 2004, 180–187

ULTRASOUND ATTENUATION IMAGING

Radovan Jiřík * — **Torfinn Taxt** ** — **Jiří Jan** *

This paper studies imaging of tissue-specific ultrasound attenuation. A new method is presented where the imaged parameter is the mean attenuation coefficient between the probe and the given pixel position. The method is based on the least-mean-squares approximation of short segments of A-scan radiofrequency signals using a physical model. The parametric image shows some of the tissue structures. It can also be used as a preliminary step in estimation of the ultrasound attenuation coefficient. Furthermore, the mean attenuation coefficient is a parameter influencing the space-variant ultrasonographic point spread function, so it can be used to improve the spatial resolution of ultrasound image through deconvolution. Testing of the method on images of a tissue-mimicking phantom, and on clinical images of liver and thigh showed relatively good agreement of the estimated attenuation coefficients with the known reference values.

K e y w o r d s: ultrasound imaging, parametric imaging, estimation of attenuation coefficient, deconvolution of ultrasonographic images

1 INTRODUCTION

Ultrasound attenuation parameters are closely related to the type and the pathological state of the tissue [1, 2]. Therefore, the estimated attenuation parameters can be used as a feature in quantitative tissue characterization. Ultrasound attenuation is also an important factor affecting spatial resolution of ultrasound images since the higher ultrasonic frequencies are attenuated more than the lower ones [1, 2, 3]. Knowing the attenuation as a function of frequency and depth would allow estimation of the depth-dependent 1-D point spread function component caused by attenuation. Knowledge of this component can be used to improve the spatial resolution of the ultrasonic image through deconvolution.

During the last three decades, there has been a considerable interest in estimation of ultrasound attenuation parameters. Most of the published methods assume a linear frequency-dependence of the attenuation coefficient ($n = 1$, see Eq. (1)). This is approximately valid for soft tissues.

Several estimation methods are based on the downward shift of the mean frequency of the radiofrequency signal as a result of attenuation. In [4], the mean frequency is estimated using the short time Fourier transform, while in [5, 6, 7] parametric models (*eg* AR model) of the processed radiofrequency signal segment are introduced, followed by subsequent spectral analysis. Another approach to estimate the mean frequency is based on the autocorrelation function [6].

In [2], the attenuation coefficients are estimated for each discrete frequency, using a short time Fourier analysis, and the estimates are fitted to a line, following a linear dependence of the attenuation coefficient on frequency.

A different approach to estimation of the attenuation coefficient, based on depth dependent statistical characteristics of the radiofrequency signal, is presented in [8]. In [9], the attenuation profiles are estimated, based on a least-mean-squares approximation of A-scan radiofrequency signal corresponding to a layered tissue model.

Generally, the tissue has a slightly nonlinear frequency-dependent attenuation coefficient ($n \approx 1.0$–1.3) [10]. The nonlinear frequency-dependence of the attenuation coefficient is considered in [11], where a series expansion of the attenuation coefficient is estimated using moments of the amplitude spectra at different depths. In [3], the received signal is filtered by a bank of narrow bandpass filters and the attenuation coefficients at each filter center frequency are calculated, using a time-domain method. The frequency dependence (the power n of Eq. (1)) of the attenuation coefficient is then estimated using maximum-likelihood estimation.

The published methods, except for [9], estimate the attenuation coefficient only in large areas with presumably constant attenuation properties. To our knowledge, no method has been published capable to provide detailed images of the attenuation coefficient of heterogeneous tissues on a pixel-by-pixel basis (for each pixel of a B-mode ultrasonic image). In contrast, this paper introduces a method for tracking the attenuation coefficient in B-mode ultrasonic images on a pixel-by-pixel basis. The resulting parametric images show the mean attenuation coefficient between the probe and the given pixel position; this quantity is later referred to as the cumulative attenuation coefficient. The ultrasound attenuation imaging is based on analyzing short segments of ultrasonic radiofrequency signals separately.

The parametric images show some of the tissue structures. In selected regions of the parametric images, the local tissue-specific attenuation coefficient is estimated and compared with reference values. The method can also provide information on the attenuation part of the 1-D point

* Department of Biomedical Engineering, Brno University of Technology, Kolejní 2906/4, 61200 Brno, Czech Republic, E-mail: jirik@feec.vutbr.cz

** Dept. of Biomedicine, University of Bergen, Jonas Lies vei 91, 5009 Bergen, Norway, E-mail: Torfinn.Taxt@fys.uib.no

ISSN 1335-3632

spread function and thus, allows removing this blurring part by means of deconvolution.

The proposed method was tested on images of a tissue-mimicking phantom, liver and thigh. The estimated local attenuation coefficients were mostly in accordance with the literature values.

The paper is organized as follows. In Section 2, one-dimensional radial models of radiofrequency signal are described. A new method for tracking the attenuation coefficient in ultrasonographic images is presented in Section 3. Section 4 contains a description of the recorded images and the used parameter values. In Section 5, experimental results are described. Finally, the significance and limitations of the presented method are discussed in Section 6.

2 MODELS OF ATTENUATION

The radiofrequency signal recorded at the ultrasonic probe depends on many factors, including the transmitting and receiving electrical circuits, the transducer geometry, piezoelectric properties of the transducer and the composition of the interrogated tissue. In this section, one-dimensional radial models of radiofrequency signal for homogeneous and heterogeneous regions are reviewed.

2.1 Homogeneous tissue region

The spectrum of the returned signal $S(\omega, d)$, recorded at the probe and corresponding to the depth d, can be modeled as a product of several transfer functions:

$$S(\omega,d) = A(\omega)\cdot H(\omega)\cdot D(\omega,d)\cdot e^{-2\alpha d-2\beta d|\frac{\omega}{2\pi}|^n+i\phi(\omega,d)}\cdot R(\omega,d)\,. \quad (1)$$

In this model, d is the distance between the probe and the given region. $A(\omega)$ denotes the electrical signal applied to the input of the transducer. $H(\omega)$ corresponds to the electroacoustical round-trip transfer function of the transducer, which is given by its design characteristics. $D(\omega, d)$ describes the diffraction effects, which are caused by the finite extent of the transducer [12, 13]. $R(\omega, d)$ is the tissue characterising function, depending on the characteristics and the distribution of the diffuse scatterers and specular reflectors situated in the irradiated area at the depth d. It is a highly irregular composite function of position and frequency [14]. The exponential term represents the attenuation transfer function. Here, α denotes the frequency independent attenuation coefficient and β the frequency dependent attenuation coefficient [1, 15]. n determines the degree of frequency dependence of the attenuation. For most soft tissues, the value of n is close to one, meaning the linear dependence. The linearity is assumed in our approach too. The term $\phi(\omega, d)$ denotes the phase response of the attenuation transfer function [16].

Several simplifications of the model of Eq. (1) can be made. In [4], the product of the transfer functions $A(\omega)$, $H(\omega)$ and $R(\omega, d)$ is approximated by a Gaussian shaped spectrum. In the present paper, a Gaussian shaped spectrum $G(\omega)$ centered at the mean frequency of the probe is used to model the product $A(\omega)\cdot H(\omega)$.

The diffraction phenomenon affects mainly the near field of the transducer. Assuming that the interrogated tissue is located in the far-field region, the diffraction transfer function can be considered constant for a given depth. A composite depth dependent factor $c(d)$ reflecting the diffraction effect may be defined so that it includes also the frequency independent attenuation term and, in addition, some further factors affecting all frequency components to the same extent (e.g. time gain compensation, apodization).

After the simplifications, the model has the following form:

$$S(\omega,d) = c(d)\cdot G(\omega)\cdot e^{-2\beta d|\frac{\omega}{2\pi}|+i\cdot\phi(\omega,d)}\cdot R(\omega,d)\,. \quad (2)$$

2.2 Heterogeneous Tissue Regions

A heterogeneous region is assumed to consist of several (K) layers of homogeneous tissue, having thicknesses d_i and attenuation coefficients α_i, β_i, $i = 1, ..., K$. The model (2) can be generalized to a model of heterogeneous regions:

$$S(\omega,d) = c(d)\cdot G(\omega)\cdot e^{-2|\frac{\omega}{2\pi}|\sum_i \beta_i d_i+i\cdot\phi(\omega,d)}\cdot R(\omega,d)\,. \quad (3)$$

Applying the model (2) to data recorded from a heterogeneous region in the time corresponding to the depth d_k, the coefficient β in Eq. (2) corresponds to the mean frequency-dependent attenuation coefficient of the tissue between the probe and the given depth d_k. Let us define this value as the cumulative attenuation coefficient and denote it $\overline{\beta_k}$. The word "cumulative" stands for cumulation (summation) of the terms $(\beta_i \cdot d_i)$ along the beam, which is used in derivation of $\overline{\beta_k}$. Below, the relationship between the cumulative attenuation coefficient and the local attenuation coefficient is derived.

Divide the A-scan radiofrequency signal into small segments of a constant thickness Δ, where Δ is the depth increment corresponding to the distance of two adjacent samples of the recorded radiofrequency signal. The attenuation coefficient within each small segment is supposed constant. Comparison of the models for homogeneous and heterogeneous regions (Eqs. (2) and (3)) then leads to

$$\overline{\beta_k} d_k = \sum_{i=1}^{k} \beta_i \Delta\,. \quad (4)$$

Consider a small homogeneous area with the attenuation coefficient β, lying in a heterogeneous tissue. For the cumulative attenuation coefficients at the depths d_k and d_{k+n} within this homogeneous area, it follows that

$$\overline{\beta_{k+n}} d_{k+n} = \overline{\beta_k} d_k + n\beta\Delta\,. \quad (5)$$

This relation shows that for a homogeneous area the term $\overline{\beta_k} d_k$ depends linearly on the depth index k with the slope $\beta\Delta$. Based on this fact, a method is derived to estimate the local attenuation coefficient within a homogeneous area from a cumulative-attenuation-coefficient image: First, a modified parametric image is formed by multiplying each pixel of the cumulative-attenuation-coefficient image by the corresponding depth. Then, a homogeneous rectangular area of the modified parametric image is selected and the beams of this area are averaged. The local attenuation coefficient is estimated by applying linear regression to the average sequence. The slope estimated within the given homogeneous region corresponds to the local attenuation coefficient of the given tissue.

3 ESTIMATION OF CUMULATIVE ATTENUATION COEFFICIENT

This section describes the method for estimation of the cumulative attenuation coefficient using a model of the radiofrequency signal in the log spectrum domain. Each A-scan signal is first divided into small overlapping segments. Each of them is weighted by a Hamming window to reduce the ringing artifacts. Then, the signal is zero-padded to increase the sampling density of the spectrum estimates. Finally, the magnitude spectrum and the corresponding log spectrum are computed.

Considering only the attenuation term and the transducer excitation with its round-trip electroacoustical transfer function, $|G(\omega)|$, the magnitude spectrum of a segment at the depth d_k can be modelled, according to Eq. (2), as

$$|S(\omega, d_k)| = c(d_k) e^{-\frac{(\omega-\omega_0)^2}{2\sigma^2}} e^{-2\overline{\beta_k} d_k |\frac{\omega}{2\pi}|}, \qquad (6)$$

where ω_0 and σ^2 are parameters specific for the applied transducer: ω_0 is the transducer center frequency and σ^2 specifies the bandwidth of the transmitted ultrasound pulse. $c(d_k)$ represents a constant factor corresponding to the depth d_k (including the frequency-independent attenuation term), the first exponential factor is the Gaussian shaped spectrum $|G(\omega)|$ from Eq. (2). The second exponential factor models the frequency-dependent attenuation.

The σ parameter is estimated from the recorded radiofrequency signal. According to [17], the Gaussian-shaped ultrasound pulse spectrum exhibits a change of the mean frequency with depth, but the bandwidth, *ie* the σ parameter, remains unchanged (in the case of linear frequency-dependence of the attenuation coefficient, *ie* n=1 in Eq. (1)). The estimate of the ultrasound pulse spectrum is calculated by averaging spectra of several adjacent beam segments. Assuming a Gaussian shape of the ultrasound pulse spectrum, the amplitude spectrum width at the level 0.6 of the normalized amplitude spectrum corresponds to 2σ.

The logarithmic transform of Eq. (6) gives

$$\log|S(\omega, d_k)| = \log c(d_k) - \frac{(\omega-\omega_0)^2}{2\sigma^2} - 2\overline{\beta_k} d_k |\frac{\omega}{2\pi}|. \qquad (7)$$

Denoting $\log c(d_k)$ as C_k, there are two unknowns $\overline{\beta_k}$ and C_k. They are estimated from the log spectrum of the kth segment, using least-mean-squares (LMS) approximation.

To avoid the problem of spectral values close to zero where the logarithm is undefined, a small constant is added to the spectrum amplitude before the logarithmic transform is applied.

Not all values of the discrete log spectrum are used in the LMS fitting. In the frequency bands close to zero frequency and to the Nyquist frequency the signal to noise ratio is low due to the band limited transfer function of the ultrasound transducer. Thus, the outer frequency bands are not considered in the LMS fitting. The used frequency band is estimated from the recorded radiofrequency signal. Approximating the log spectrum of a beam segment by Eq. (7) corresponds to addition of the term $\frac{(\omega-\omega_0)^2}{2\sigma^2}$ to the log spectrum of the beam segment with subsequent linear regression applied to the modified log spectrum. In the ideal case, the modified log spectrum would be a linear function of frequency. This is not true in the outer frequency bands. The useful frequency range is estimated as the frequency band with linear trend, based on the average modified log spectrum of several adjacent beam segments. This is done visually, before any computation. As the mean frequency of the radiofrequency signal varies with depth, the frequency range changes as well. To keep the simplicity of the approach, the range is determined as the frequency band exhibiting a linear trend in the whole depth span of the image.

In this model, the tissue characterising function $|R(\omega, d)|$ is not considered. It is supposed to be a random rapidly changing frequency-domain function, causing a scalloped spectrum. A similar effect of the tissue characterising function is also expected in the log spectrum domain [18, 19]. These rapid changes are averaged out by the least-mean-squares approximation. The pseudocode of the procedure is shown in Algorithm 1.

Algorithm 1 Estimation of the cumulative attenuation coefficient in log spectrum domain

```
1: for all beams b do
2:   Divide to overlapping segments
3:   for all segments s do
4:     Weighting by a Hamming window
5:     Zero-padding
6:     FFT
7:     Derive amplitude spectrum as abs. values
8:     Add a small constant
9:     Logarithmic transform
10:    LMS fitting of the log spectrum by the Eq. (7)
       to find β̄_{b,s}
11:  end for{for all segments s}
12: end for{for all beams b}
```

It should be noted that the this method of estimating the cumulative attenuation coefficient is not affected by the time gain compensation, which only compensates for the frequency-independent attenuation by amplifying all frequency components at the given depth by the same factor.

4 IMAGE DATA AND PARAMETER VALUES

To assess the accuracy of the presented method of ultrasound attenuation imaging, it was tested on recorded quadrature data of image sequences.

Three image sequences were recorded: of a tissue mimicking phantom, a liver and a thigh cross-section. All image sequences were recorded with GE Vingmed Ultrasound System 5 scanner. Raw radiofrequency signals after correction of the depth-dependent frequency-independent attenuation (time gain compensation) and after quadrature demodulation were recorded and used as the input to the subsequent image processing. The recorded quadrature signal is a complex-valued analytic signal with an asymmetrical spectrum centered around the transmitter center frequency. The quadrature signal can be used in place of the original radiofrequency signal without any modifications of the algorithm.

The phantom images were acquired using a precision multi-purpose grey scale phantom Gammex 403GS. The phantom contains gray scale and point targets in a uniform tissue-mimicking gel of properties very close to human liver. The attenuation coefficient of the tissue-mimicking gel was 0.7 ± 0.05 dB/cm/MHz.

Phased array probe fpa_64_2.5_c with a nominal frequency of 2.5 MHz and 64 elements was used. The demodulation frequency of the recorded quadrature signal was 2.2 MHz and the sampling frequency 3.3 MHz (after quadrature demodulation).

A sequence of 16 images was recorded from the deeper part of the phantom to avoid the effect of diffraction, which significantly affects the spectrum of the radiofrequency signal in the near-field. The images consisted of 78 beams, each one of 494 samples corresponding to a depth span of 6.7 cm to 18.1 cm. The angle increment between the neighbouring beams was 0.02 rad.

To test the algorithm on clinical images, two in-vivo image sequences were recorded, a sequence of liver and of the thigh muscle. Curved linear probe cla_192_3.5 with a nominal frequency of 3.5 MHz and 192 elements was used. The demodulation frequency of the recorded quadrature signal was 3.3 MHz and the sampling frequency 4 MHz (after quadrature demodulation).

Each sequence included 10 images. The size of the liver images was 114 beams (lateral direction) and 284 samples in the axial direction, corresponding to the depth span of 6.8 cm to 12.3 cm. The angle increment between the neighboring beams was 0.007 rad. The size of the thigh images was 114×232 pixels in the lateral and axial direction, respectively (depth span 5.0 cm to 9.5 cm), angle increment 0.007 rad.

The parameter σ of the least-mean-squares approximation (Eq. (7)) was estimated from the average amplitude spectrum of all beam segments corresponding to the same depth. The estimates at 5 various depths were averaged. For phantom images $\sigma = 0.7$ MHz and for the liver and thigh images $\sigma = 0.6$ MHz. The frequency band of the log spectrum values used in the LMS fitting was 1.3 to 3.2 MHz (the whole frequency range of the quadrature signal: 0.6 to 3.9 MHz) for the phantom images, 2.3 to 4.5 MHz for the images of liver, and 1.6 to 4.1 MHz for the images of thigh (the whole frequency range for both clinical image sequences: 1.3 to 5.3 MHz).

To find the optimum segment length in the algorithm for estimation of the cumulative-attenuation coefficient (Algorithm 1), various segment lengths were tested on the phantom images: 8, 16, 32 and 64 pixels. The overlaps were 7, 15, 31 or 63 pixels, respectively, to provide an attenuation-coefficient estimate for every pixel (except for the leading and terminal beam samples). For the images of liver and thigh, the beams were divided into segments of 16 pixels with an overlap of 15 pixels. For all sequences, the segments, weighted by a Hamming window, were zero-padded to 128 pixels.

To relate the used segment lengths to the physical parameters of the ultrasound data acquisition, the size of the ultrasound pulse was roughly estimated: First, the spectra of quadrature signals were averaged through all beams of the image, giving a rough estimate of the bandwidth, which is mainly limited by the ultrasound pulse. Supposing a smooth spectrum of the pulse, the resulting amplitude spectrum was smoothed (using a Butterworth filter) to suppress the tissue characterising component (Eq. (2)). Finally, the inverse Fourier transform was applied, giving a rough estimate of the pulse. The width of the pulse estimate, measured at 50% height of its envelope, was 4 pixels (0.9 mm) for the phantom images and 3 pixels (0.6 mm) for images of liver and thigh.

5 RESULTS

The accuracy of the presented method was assessed by comparing the obtained results with the known attenuation coefficients characteristic for the selected phantom and the imaged tissues. Since reference values are available only for the local attenuation coefficients, these local values had to be estimated from the parametric images of the cumulative attenuation coefficient, as derived in Section 2.2.

5.1 Phantom Images

An example of the modified log spectrum used for the estimation of the used frequency band is given in Fig. 1. The plot illustrates the higher variance of the modified log spectra in the outer frequency bands due to the limited band of the transducer. The low values of the modified log spectra in these bands indicate that the further from the

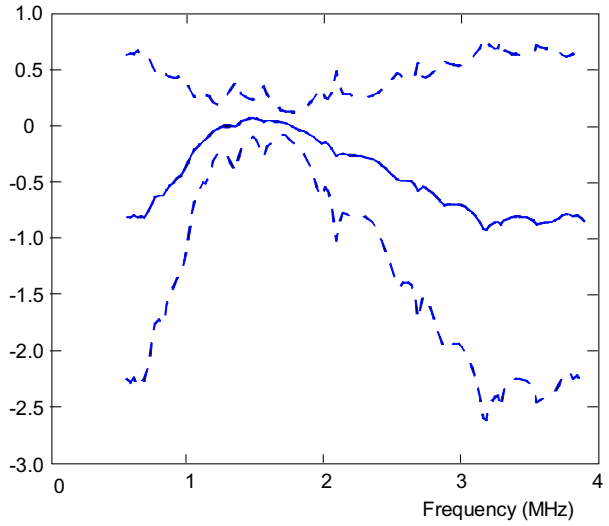

Fig. 1. Example of the modified log spectrum (phantom image). The solid curve shows the average of 50 adjacent segments of one beam, the dashed curves are one standard deviation up and down from the mean. Segment length 16, overlap 15, zero-padded to 128 samples. The frequency axis corresponds to the signal before the quadrature demodulation.

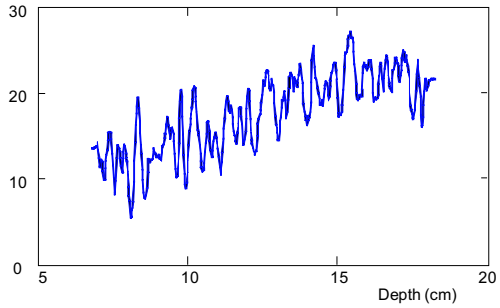

Fig. 2. Example plot of parametric image beams, with the parameter being the cumulative attenuation coefficient multiplied by depth; average of 4 beams, segment length 16.

Table 1. Estimates of the local attenuation coefficient of the phantom image sequence, in dB/cm/MHz (mean ± std. dev.)

Region size (ax. dir.) Segment size (pixels)	80	160	320
8	0.7 ± 1.3	0.5 ± 0.4	0.6 ± 0.1
16	0.7 ± 1.2	0.6 ± 0.4	0.7 ± 0.1
32	0.6 ± 1.0	0.6 ± 0.4	0.7 ± 0.1
64	0.7 ± 0.9	0.6 ± 0.4	0.7 ± 0.1

center frequency, the faster the real transducer amplitude response decays than a Gaussian function does.

For the phantom images, the estimated local attenuation coefficient was compared to the attenuation coefficient of the tissue mimicking gel, given in the phantom specification as 0.7 ± 0.05 dB/cm/MHz. The local attenuation coefficient was estimated from the cumulative attenuation coefficient image in homogeneous regions which included only the tissue mimicking gel, with no targets. The size of the regions was 4 beams in the lateral direction. To test the robustness of the estimates, various region sizes in the axial direction were tested: 80, 160 or 320 pixels. The mean and standard deviation of the local attenuation coefficient were calculated through all images of the phantom sequence and all region positions. The region positions were selected to cover (without overlapping) a homogeneous area of the size 320×16 pixels in the axial and lateral direction ($6.2\,\text{cm} \times 0.32$ rad).

A typical plot of averaged 4 beams of the modified parametric image (cumulative attenuation coefficient multiplied by depth) is shown in Fig. 2. The beams of the modified parametric images should be monotonic increasing, in the ideal case. As shown in the image, the beams are rather noisy, which is the result of fairly high variance of the cumulative-attenuation-coefficient estimates. However the linear trend, expected in a homogeneous tissue region, is clearly visible.

The results (Tab. 1) show the effect of the size of the homogeneous region where the local attenuation coefficient is estimated. The range mean ± standard deviation in Tab. 1 includes the correct range 0.7 ± 0.05 dB/cm/MHz of the local attenuation coefficient specific for the phantom, except for one combination of parameters (segment size 8, axial region size 320). As expected, a larger region size results in more robust estimates with lower variance. A reasonable variance of the estimates was achieved for the axial region size 320 pixels.

The results indicate that the estimation of the cumulative attenuation coefficient performs well for segment size 16, 32 and 64. The segment size of 8 pixels seems to be insufficient for estimating spectrum at the given depth. On the other hand, the parametric images calculated using long segment size are blurred in the axial direction.

5.2 Clinical Images

The results obtained with images of liver and thigh are shown in Fig. 3. The input images (Fig. 3 a,b) are shown as envelope images before format conversion from polar to Cartesian coordinates. Hence, the geometry is slightly distorted. The beams are oriented horizontally with the depth increasing from left to right. The cumulative attenuation coefficient images of liver (Fig. 3 c) had a fairly homogeneous character. The cumulative attenuation coefficient images of thigh (Fig. 3 d) showed, to a certain extent, the underlying tissue structures. The area of fat (the left area with high echogenity) exhibited fairly high variance of the estimated parameter. This character of the fat tissue has been observed earlier when measuring the attenuation coefficient in fresh human tissues [20]. The femur area (right side in the middle) was brighter, meaning higher cumulative attenuation coefficient of the

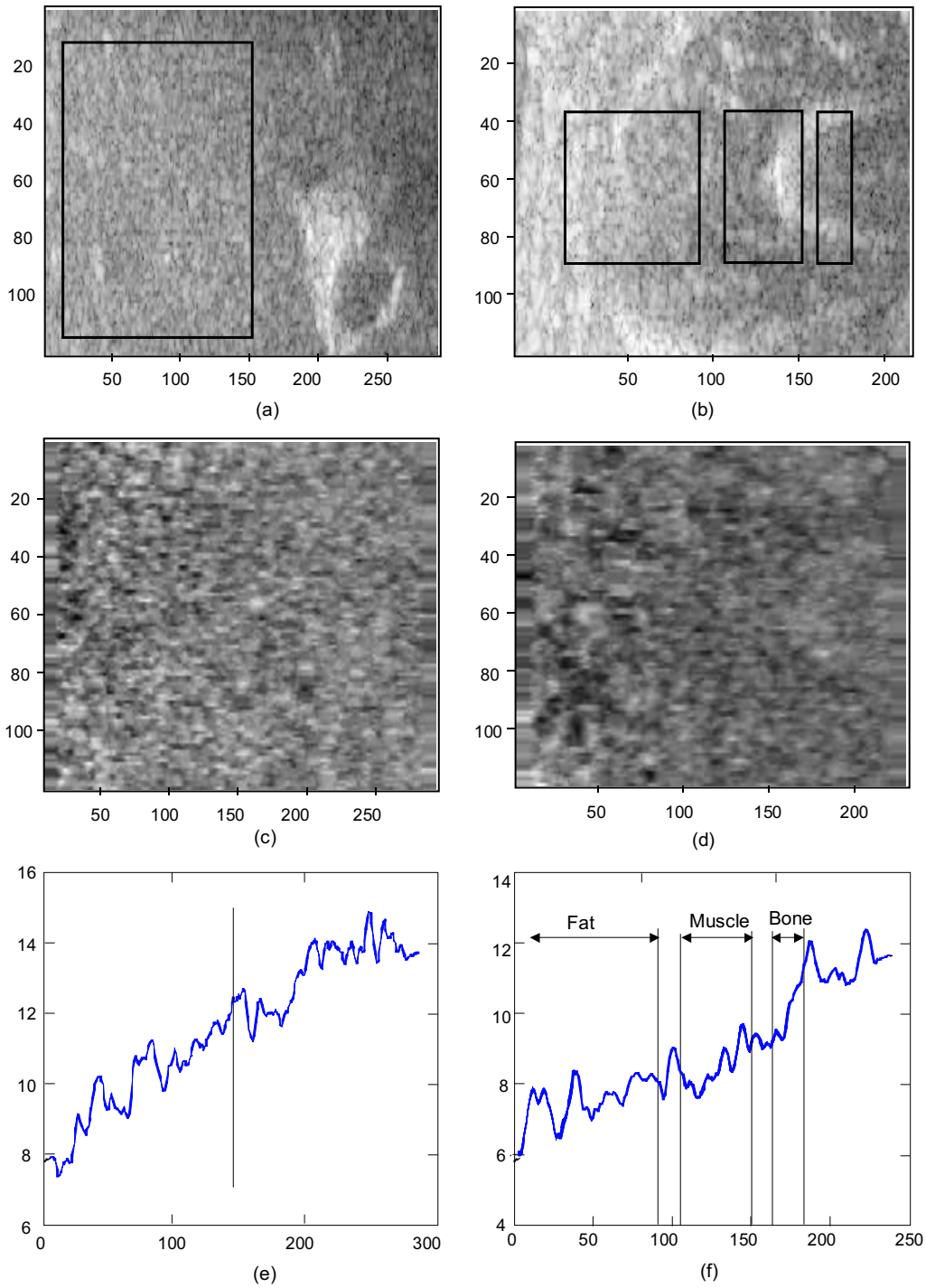

Fig. 3. Estimation of attenuation parameters. (a) envelope image of liver, (b) envelope image of thigh, (c)cumulative attenuation coefficient image of liver, (d) cumulative attenuation coefficient image of thigh, (e)estimation of the local attenuation coefficient for the image of liver, (f) estimation of the local attenuation coefficient for the image of thigh.

bone. Ultrasound wave does not penetrate inside femur, thus the inner area contained only noise. In the muscle area (between fat and femur) the cumulative attenuation estimates were fairly homogeneous.

The quantitative assessment was done using estimates of the local attenuation coefficients within homogeneous regions. The selected rectangular regions are depicted in Fig. 3 a,b. In Fig. 3 e,f the plots of averaged beams of the modified parametric images are shown (the parameter being the cumulative attenuation coefficient (Fig. 3 c,d) multiplied by depth). Only the beams crossing the used regions are considered in averaging. The vertical lines in the plots denote the borders of the regions in the axial direction. In the ideal case, the plot would be piece-wise linear with different slopes in different homogeneous regions, corresponding to the local attenuation coefficients.

The mean values and standard deviations of the local-attenuation-coefficient estimates through each sequence are summarized in Table 2.

The local attenuation coefficient values for some tissues as reported in literature (Tab. 2) vary considerably, depending on the source of information. Hence, the values give only a rough idea of the expected range. Except for fat, the estimated local attenuation coefficients were within the expected range. The reason for false estimates in the fat regions is probably the inhomogeneous character of the tissue.

Table 2. Literature values and estimates of the local attenuation coefficients, in dB/cm/MHz (mean ± std. dev.)

Tissue	Literature values			Estimated values
	[10]	[21]	[22]	
Liver	–	0.7	0.7	0.7 ± 0.0
Fat	–	0.6	0.65	0.3 ± 0.0
Muscles (normal to fibers)	1.65–1.75	1.5	1.12 (3.3)	1.2 ± 0.1
Bone	3–10	10	–	3.6 ± 0.2

6 DISCUSSION AND CONCLUSION

A method of parametric imaging based on a pixel-by-pixel estimation of the cumulative attenuation coefficient was presented. The imaged parameter shows the development of the attenuation effect with depth.

The tests on a tissue-mimicking phantom showed that the estimated local attenuation coefficient based on the calculated parametric image was in agreement with the known reference value of the phantom attenuation. Also, the parametric images estimated for real tissues gave results mostly compatible with the tissue-specific local attenuation coefficients found in literature. Furthermore, the underlying tissue structures were relatively well visible in the parametric images (in thigh images).

The resulting parametric images were fairly noisy. The main reason for the perturbations is probably the influence of the tissue characterising function which distorts the spectrum estimates. The effect was more pronounced in case of short A-scan segments used for estimation of the spectra. On the other hand, the use of long segments smoothed out the change of attenuation properties along the segment more than in case of short segments; the parametric images computed using long segments were therefore blurred in the axial direction. Thus, the segment length had to be chosen as a compromise between the robustness of the method and the spatial resolution of the attenuation images.

Another source of the method's inaccuracy is probably the diffraction effect. In the present method, its influence was neglected, assuming that the effect of diffraction in the far-field is negligible. However, even in the far field, the diffraction effect influences the spectrum of the ultrasound pulse to a small extent. The effect of diffraction on the attenuation coefficient estimation will be studied in further research.

In the present study, a linear dependence of the attenuation coefficient on frequency was supposed. This assumption is fulfilled in case of the tissue mimicking phantom and muscles [10], *ie* $n=1$ in Eq. (1). However, for fat $n=1.2$ and for liver $n=1.1$ [10] (the value of n for bones was not found in the literature). Hence, the slightly nonlinear frequency-dependence of the attenuation coefficient also contributes to the inaccuracy of the attenuation estimates.

As the imaged parameter is the mean attenuation coefficient of the tissue lying between the probe and the given point in the parametric image, the steps in the local attenuation coefficient of adjacent tissues can not be visualised as clearly as in the hypothetical image of the local attenuation coefficient. This is especially true for deeper structures, where the resulting cumulative attenuation coefficient is a result of averaging through a longer depth span and thus, the change in the local attenuation coefficient does not contribute much to the change of the cumulative attenuation coefficient. However, in the context of the research in the area of estimating the attenuation coefficient, where there has not been found any automatic method for generating local-attenuation-coefficient images yet, the presented method can be considered a step towards attenuation parametric imaging.

The presented parametric images of the cumulative attenuation coefficient can be used as a preliminary step in estimation of the local attenuation coefficient. So far, the presented parametric images allow for estimation of the local attenuation coefficient only in fairly large homogeneous regions. To approach the estimation on a pixel-by-pixel basis, the reliability of the method has to be improved. This could be done, for example, by incorporating more segments into the estimation procedure, instead of estimation of the cumulative attenuation coefficient separately in each A-scan segment. This will be the subject of further research.

The parametric images of the cumulative attenuation coefficient can also be the direct input to the deconvolution of ultrasound images aiming at compensating for the distortion of the spatial resolution caused by the frequency-dependent attenuation.

In conclusion, the present method of parametric imaging has the potential to give valuable information for assessing attenuation properties of tissues and possibly for improving the spatial resolution.

Acknowledgments

The project has been supported by the Research Council of Norway, by the grant no. 102/02/0890 of the Grant Agency of the Czech Republic and by the grant no. 1K03017 of the Czech Ministry of Education, Youth and Sports. We are also grateful to GE Vingmed Ultrasound a.s. for making the recording of raw quadrature signals

possible and to Trygve Hausken and Hans Torp for their help in recording the experimental image data.

References

[1] OOSTERVELD, B. J.—THIJSSEN, J. M.—HARTMAN, P. C.—ROMIJN, R. L.—ROSENBUSCH, G. J. E.: Ultrasound Attenuation and Texture Analysis of Diffuse Liver Disease: Methods and Preliminary Results, Phys. Med. Biol. **36** No. 8 (1991), 1039–1064.

[2] WILSON, L. S.—ROBINSON, D. E.—DOUST, B. D.: Frequency Domain Processing for Ultrasonic Attenuation Measurement in Liver, Ultrasonic Imaging **3** No. 3 (1984), 278–292.

[3] HE, P.—McGORON, A.: Parameter Estimation for Nonlinear Frequency Dependent Attenuation in Soft Tissue, Ultrasound in Med. & Biol. **15** No. 8 (1989), 757–763.

[4] FINK, M.—HOTTIER, F.—CARDOSO, J. F.: Ultrasonic Signal Processing for in Vivo Attenuation Measurement: Short Time Fourier Analysis, Ultrasonic Imaging **5** No. 2 (1983), 117–135.

[5] SHIH, L. Y.—BARNES, C. W.—FERRARI, L. A.: Estimation of Attenuation Coefficient for Ultrasonic Tissue Characterisation Using Time-Varying State Space Model, Ultrasonic Imaging **10** No. 2 (1988), 90–109.

[6] LYMBERIS, A.—HERMENT, A.—DEMOMENT, G.—FRIC, C.: Estimation of Frequency-Dependent Attenuation Based on Parametric Spectral Analysis and Correlation Lags of the Demodulated Echo Signal, Ultrasonic Imaging **13** No. 1 (1991), 1–26.

[7] GIRAULT, J. M.—OSSANT, F.—OUAHABI, A.—GUITTET, C.—KOUAMÉ, D.—PATAT, F.: Non-Stationary Parametric Spectral Estimation for Ultrasound Attenuation, Acoustical Imaging **23** (1997), 53–59.

[8] JANG, HEUNG S.—SONG, TAI K.—PARK, SONG B.: Ultrasound Attenuation Estimation in Soft Tissue Using the Entropy Difference of Pulsed Echoes between Two Adjacent Envelope Segments, Ultrasonic Imaging **10** No. 4 (1988), 248–264.

[9] MÍŠEK, A.—JAN, J.: Deriving Attenuation Profiles from Raw Digital Ultrasonographic Data, J. Electrical Engineering **53** No. 3-4 (2002), 70–75.

[10] ANGELSEN, B.: Ultrasound Imaging — Waves, Signals, and Signal Processing, Emantec AS, 2000.

[11] CLOOSTERMANS, M. J.—VERHOEF, W. A.—THIJSSEN, J. M.: Generalized Description and Tracking Estimation of the Frequency Dependent Attenuation of Ultrasound in Biological Tissues, Ultrasonic Imaging **7** No. 4 (1985), 133–141.

[12] O'DONNELL, M.: Effects of Diffraction on Measurements of the Frequency-Dependent Ultrasonic Attenuation, IEEE Trans. Biom. Eng. **30,** No. 6 (1983), 320–326.

[13] KUC, R.—REGULA, D. P.: Diffraction Effects in Reflected Ultrasound Spectral Estimates, IEEE Trans. Biom. Eng. **BME-31** No. 8 (1984), 537–545.

[14] LAUGIER, P.—BERGER, G.—FINK, M.—PERRIN, J.: Specular Reflector Noise: Effect and Correction for in Vivo Attenuation Estimation, Ultrasonic Imaging **7** No. 4 (1985), 277–292.

[15] FORSTER, F. K.—GUTTORP, P.—GOW, E. L.: Variance Reduction for Ultrasonic Attenuation Measurements from Backscatter in Biological Tissue, IEEE Trans. Sonics Ultrasonics **SU-32** No. 4 (1985), 523–530.

[16] GURUMURTHY, K. V.—ARTHUR, R. M.: A Dispersive Model for the Propagation of Ultrasound in Soft Tissue, Ultrasonic Imaging **4** No. 4 (1982), 355–377.

[17] KUC, R.—SCHWARTZ, M.—von MINSKY, L.: Parameter Estimation of the Acoustical Attenuation Coefficient Slope for Soft Tissues, in IEEE Ultrasonics Symposium, 1976,.

[18] TAXT, T.—JIŘÍK, R.: Superresolution of Ultrasound Images Using the 1st and 2nd Harmonic Signal, IEEE Trans. Ultrason. Ferroelec. Freq. Cont. **51** No. 2 (2004), 163–175.

[19] JIŘÍK, R.: Restoration and Analysis of Ultrasonic Images, PhD thesis, Brno University of Technology, 2004.

[20] BAMBER, J. C.: Ultrasonic Attenuation in Fresh Human Tissues, Ultrasonics **19** No. 4 (1981), 187–188.

[21] EVANS, D. H.—McDICKEN, W. N.—SKIDMORE, R.—WOODCOCK, J. P.: Doppler Ultrasound — Physics, Instrumentation, and Clinical Applications, John Wiley & Sons, 1989.

[22] MACOVSKI, A.: Medical Imaging Systems, Prentice-Hall, Inc., 1983.

Received 7 May 2004

Radovan Jiřík, born in 1976. MSc (1999) in Cybernetics, Control and Measurement (Brno University of Technology). PhD (2004) in biomedical engineering (Brno University of Technology). Currently researcher/teacher at Brno University of Technology, Department of Biomedical Engineering. Research interests: ultrasonic imaging, image restoration, image and signal processing.

Torfinn Taxt, born in 1950, professor of Biomedical Imaging and Analysis at the University of Bergen and senior staff member at the Dept. of Radiology, Haukeland University Hospital, Bergen, Norway. He has a PhD degree in developmental neuroscience (1983) and MD (1976) and MSc (1978) degrees in computer science from the University of Oslo. He is Associate Editor of IEEE Medical Imaging. His primary research interests are restoration, segmentation, and multispectral analysis applied to magnetic resonance and medical ultrasonic images. He has also published papers on image models, satellite remote sensing, sonars, and document processing. T. Taxt has published about 75 international publications in neuroscience, image processing, and pattern recognition.

Jiří Jan, born in Brno (Czechia) in 1941, MSc in Electrical Engineering (University of Technology Brno 1963), PhD in radioelectronics (1969), full professor of electronics at the University of Technology Brno (1991). Presently, Head of the Department of Biomedical Engineering and coordinator of the Institute for Signal and Image Processing, both of the Faculty of Electrical Engineering and Communication, UT Brno. Associate Editor of IEEE Transactions on Biomedical Engineering (1996–2001), guest editor of the special issue of JASP (no. 4/2003) on Modality Oriented Medical Image Processing. Chair of the international committee of biennial EURASIP Biosignal conference. He is the author of the book Digital Signal Filtering, Analysis and Restoration (IEE London 2000) and of over 200 journal and conference papers. Scientific interests: digital signal and image processing and restoration, including biomedical applications, especially in ultrasonic tomography, stereo-analysis, and image registration.